J Mol Model (2013) 19:2509–2518
DOI 10.1007/s00894-013-1789-9

ORIGINAL PAPER

Investigation by MD simulation of the key residues related to substrate-binding and heme-release in human ferrochelatase

Yaxue Wang · Jingheng Wu · Jinqian Ju · Yong Shen

Received: 17 October 2012 / Accepted: 30 January 2013 / Published online: 28 February 2013

Abstract Molecular dynamics (MD) simulations of three models based on the crystal structure of the E343K variant of human ferrochelatase were performed in this study. The "open" and "closed" conformations of the enzyme obtained by simulations are in agreement with the corresponding crystal structures. The snapshots and the structure analysis indicate that alterations of the hydrogen bonds and the positions of E347 and E351 lead to a conformational change in the π-helix. The hydrogen bonded form of residue R164 could be regarded as a signal indicating alteration of the active site conformation. When R164 forms a hydrogen bond with D95, the active site is closed, and when a hydrogen bond is formed with E171, the active site is open. Interestingly, the protoporphyrin with Fe^{2+} is observed to move noticeably out of the enzyme while the protoporphyrin lacking Fe^{2+} remains almost fixed. Alterations of the hydrogen bonds between the propionate of the heme and R115, K118 and S303 trigger movement of the heme out of the active site. Residues E347 and E351, which are located on the π-helix and form an acidic path leading to a salt bridge interaction with the propionate of the heme, accelerate the release process.

Keywords Human ferrochelatase · Protoporphyrin IX · Heme · Ferrous ion · Molecular dynamics

Electronic supplementary material The online version of this article (doi:10.1007/s00894-013-1789-9) contains supplementary material, which is available to authorized users.

Y. Wang · J. Wu · J. Ju · Y. Shen (✉)
KLGHEI of Environment and Energy Chemistry, School of Chemistry and Chemical Engineering, Sun Yat-sen University, 510275, Guangzhou, People's Republic of China
e-mail: cessy@mail.sysu.edu.cn

Y. Wang
School of College of Food Science and Engineering, Northwest A&F University, 712100, Yangling, People's Republic of China

Introduction

Ferrochelatase (protoheme ferrolyase, EC 4.99.1.1) is the terminal enzyme in heme biosynthesis and catalyzes the insertion of ferrous ion into protoporphyrin IX to form protoheme IX (heme) [1]. Heme is a cofactor included in hemo- and myoglobins, cytochromes, all aerobic organisms and the majority of anaerobes and facultative organisms. Biosynthesis of heme requires eight enzymatic steps in mammals and most fungi, and nine in plants and most bacteria. Human and bacterial ferrochelatase are highly conserved at the level of tertiary structure although there is less than 10 % conservation at the level of amino acid sequence [2]. Mutations in the human ferrochelatase gene can lead to the disease erythropoietic protoporphyria (EPP) [3, 4]. A symptom of this disease is light-sensitive dermatitis, caused by overproduction of protoporphyrin and its deposition in skin and liver. In some cases, it may even lead to fatal liver damage [5].

The mechanism of porphyrin metallation has attracted much interest and has been studied extensively by many groups in the past decades [6–13]. However, most of these studies are based on the metallation process in solution rather than in ferrochelatase. Recent works have provided some insights into the catalytic mechanism of ferrochelatase and the roles of some key residues [14–19]. Residues H263, F337, H341 and E343 in human ferrocheltase, which are located on one side of the protoporphyrin, are regarded as involving proton abstraction from protoporphyrin during catalysis [20, 21] and F337 also plays a key role on controlling the entrances to two solvent-filled tunnels located at the back of the active site pocket [16, 22, 23]. Fe^{2+} is thought to be transported from the exterior of the enzyme at D383/H231 via W227 and Y191 to the site of metallation at R164 in human ferrochelatase [10, 20] and in yeast [23]. However, in *Bacillus subtilis*, a different route is employed for ferrous ion transportation [13, 19].

Recently, Medlock et al. [14] were the first to report the crystal structure of the E343K variant of human ferrochelatase with bound protoporphyrin. By analyzing the structure, they found that the substrate-bound structure possesses a "closed" active site conformation while the substrate-free enzyme (R115L) [20] has an "open" active site. The "open" and "closed" conformations may regulate protoporphyrin binding and product release [15, 24]. The π-helix (residues 340–349) is unwound in the F110A variant [15] enzyme of bound heme. This conformational alternation from substrate-bound to heme-free should be related to some key residues playing important roles in the catalytic process of the enzyme. To better understand the catalytic mechanism of human ferrochelatase, some problems should be solved: what leads the enzyme to open and close its mouth; why does the conformation of the π-helix change when ferrous ion is imported; and which residues are involved in the substrate entering and exiting the active site pocket. To answer these questions, experimental results are not enough. In this paper, we performed a series of molecular dynamics (MD) simulations on three models of human ferrochelatase. The snapshot details and structural rearrangements presented herein significantly advance our understanding of the substrate-binding mode and the process of product release.

Computational procedure

MD simulations are used widely in the study of protein structure and are regarded as a very useful tool with which to study the conformational changes of proteins [25–28]. In this study, we started from the crystal structure E343K (PDB code 2HRE, resolution 2.5 Å) [14] and performed MD simulations at room temperature. The different model systems considered in this study were (A) E343K without protoporphyrin, (B) E343K with protoporphyrin, and (C) E343K with metallated protoporphyrin. MD simulations were performed using the AMBER [29, 30] package with the 1999 force field [31]. The parameter files and the electrostatic potential (ESP) charge of the porphyrin and heme were generated using Turbomole software [32] at the level of BP86/6-31 G* for all atoms (Fe was described by the DZpdf basis set) [33]. The pressure was controlled at 1 atm and the temperature was maintained at 300 K. A cutoff for the nonbonded interactions of 10 Å was employed.

Before energy minimization, residue K343 was replaced with residue E343. All residues were assumed to be in their most stable protonation states at neutral pH. All Arg and Lys residues were considered to be in a protonated state, whereas all Asp and Glu residues were considered to be in a deprotonated state. After a detailed study of the surroundings and possible hydrogen-bond networks around the His residues, it was decided that His167 and His388 were protonated on the $N^{\delta 1}$ atom, His230 was protonated on the $N^{\varepsilon 2}$ atom, and the remaining His residues were doubly protonated. Protons were added using the leap module of AMBER. The [2Fe-2S] cluster was modeled as follows: Fe^{2+} is coordinated with two S atoms in the middle and the two S atoms of the Cys residues. A bond was set between the Fe and the S atom using the bond command. Each model was solvated with a 9-Å octahedral periodic water box. To neutralize the systems, 7, 5 and 5 Cl^- ions were added to systems A, B and C, respectively. Finally, the simulation system for model A is composed of a total of 5,803 protein atoms and 10,872 solvent molecules, model B contains 5,877 protein atoms and 10,869 solvent molecules, and model C consists of 5,876 protein atoms and 10,869 solvent molecules.

All the hydrogen atoms and water molecules were first equilibrated by a simulated annealing molecular dynamics calculation, followed by 10,000 steps of energy minimization. Constant volume and pressure simulations were then performed for 20 ps, respectively. Next, constant pressure equilibration by main chain restraining for 50 ps, and constant volume equilibration by main chain restraining for 200 ps were performed. The analysis of energy parameters revealed that the systems were well equilibrated. A MD run of 15 ns with a time step of 2 fs was then carried out for all systems. The trajectory was saved every 1 ps, and a total of 15,000 snapshots was taken in a production run for detailed analysis. The results were visualized using the VMD package [34] and Discovery studio 2.0. Various parameters derived from the simulations are described in the following section.

Results

Stability and flexibility of the protein structures

MD simulation was carried out within 15 ns. Figure 1a shows the root mean square deviations (RMSDs) from the crystal structures for CA, C, N atoms versus simulation time. We used the first structure of the simulation as the reference structure in the calculation of the backbone RMSD. As shown in Fig. 1a, after about 11 ns, the RMSD of each system tends to be convergent, indicating that the system becomes stable. The root mean square fluctuation (RMSF) from the averaged structure provides another approach to evaluate the convergence of the dynamic properties of the system. Figure 1b–d shows the atomic fluctuations averaged over residues for the three systems derived from the 15 ns MD trajectories. For comparison, the corresponding values of RMSF obtained from the experimental B factors in crystal structures are also shown in Fig. 1c. The experimental B factors are transformed to the RMSF with the formula $<\Delta r_i^2>=3B_i/(8\pi^2)$ [35]. The RMSF

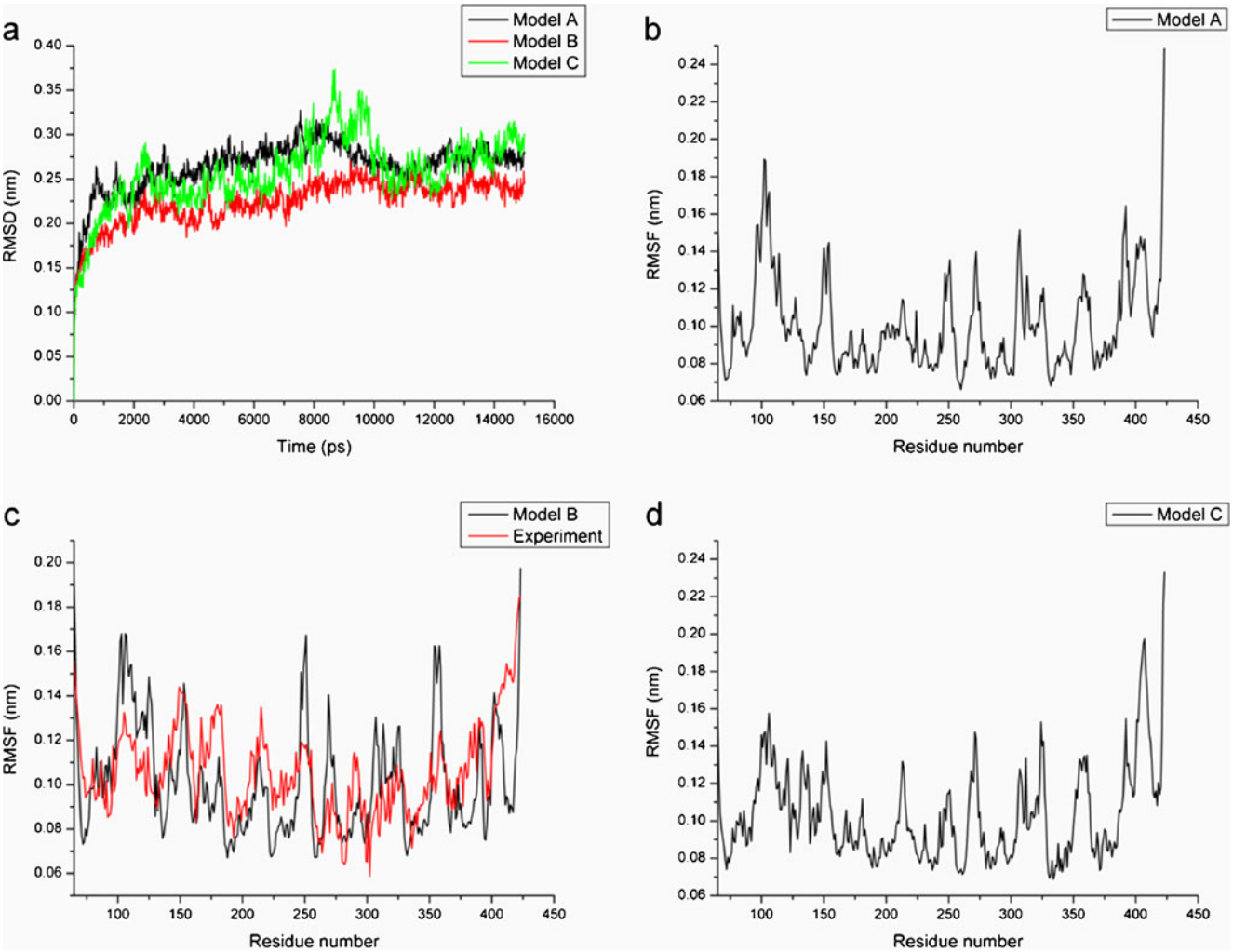

Fig. 1 **a** Time dependence of the root mean square deviations (RMSDs) from the crystal structures of human ferrochelatase and its substrate complexes for the CA, C, and N atoms in 15-ns molecular dynamics (MD) simulations. **b**–**d** Residue fluctuations obtained by averaging atomic fluctuations over the 15-ns simulation (*black curves*) for model A (**b**), B (**c**), and C (**d**) and by computing the value from the experimentally derived B factors (*red curve* in **c**)

profile is in agreement with the experimental results reflected by the B factors derived from X-ray crystallographic data, indicating that the MD results are reasonable.

General conformation description of the overall protein and substrate

The initial models for MD simulation were based on the crystal structure of E343K variant of human ferrochelatase with the protophyrin bound, which has a so-called "closed" active site. The upper "lip" of the mouth is formed by residues 90–130 while the lower "lip" is composed of residues 300–311 (as shown in Fig. 2a) [20]. The porphyrin ring and nearby residues on the active site pocket are shown in Fig. 2b–d.

The initial structure of model A was built from the crystal structure of human ferrochelatase (E343K) by removing the substrate (protoporphyrin). As a result, the first structure of the protein should be in a "closed" state. After 15 ns MD simulation the enzyme possesses an open active site conformation similar to that observed for the R115L variant [20]. Both the lower and upper lips experience large movement and the distance between them increases from 5 Å to 11 Å (Fig. S1). A cross-section of the upper and lower lip of human ferrochelatase is illustrated in Fig. 3a. The conserved π-helix is "unwound" from residues 340 to 351 (Fig. 4a).

Model B was built directly from the crystal structure of the E343K variant. The active site pocket is still closed after 15 ns of MD simulation. A cross-section of the upper and lower lip of human ferrochelatase is illustrated in Fig. 3b. Both the lower and upper lips are almost in their original sites and the distance between them stays fixed at around 5 Å (Fig. S2). The conserved π-helix exhibits no obvious change (Fig. 5a). A plot of the RMSD of the protoporphyrin

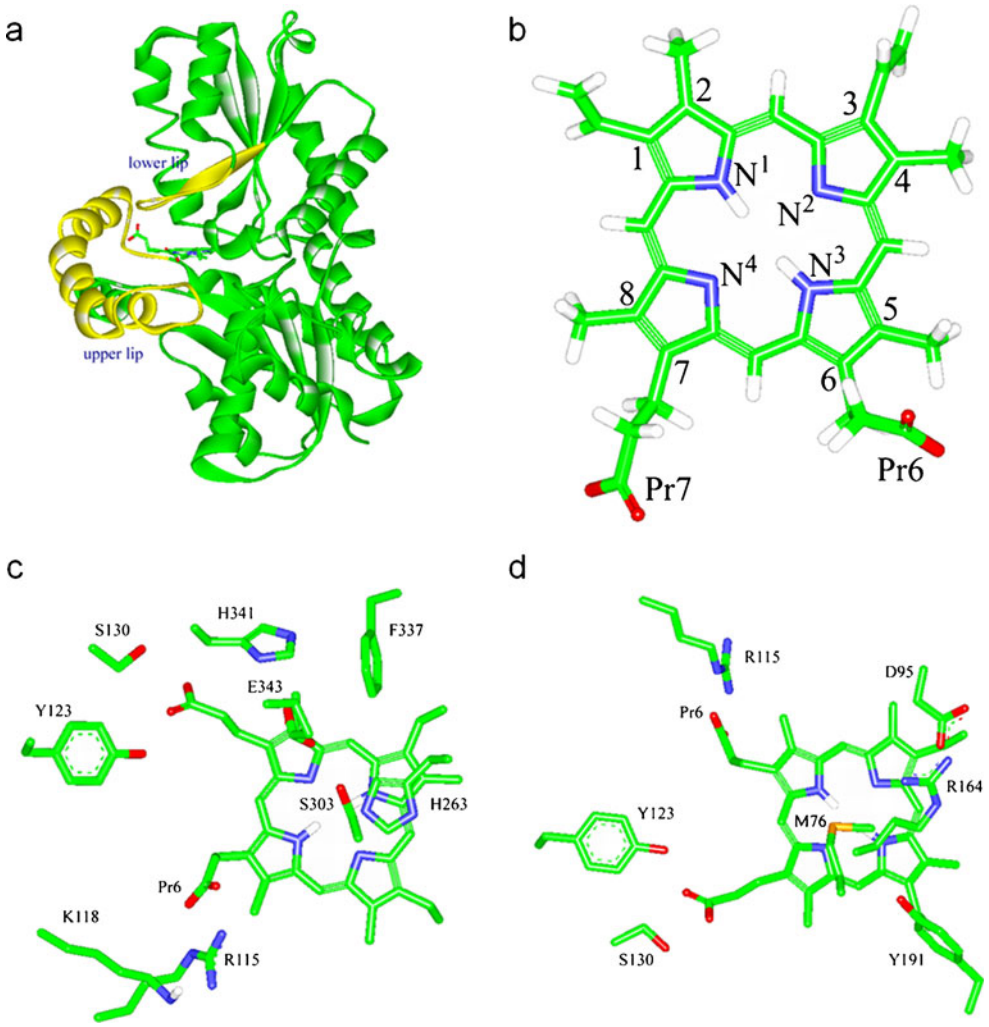

Fig. 2a–d Substrate binding to the E343K variant of human ferrochelatase. **a** Cartoon representation of the crystal structure E343K is shown in *green*, the upper and lower "lip" regions of the mouth have been highlighted in *yellow*. **b** Sticks representation of protoporphyrin IX. The "Pr6" and "Pr7" mean the propionate at position 6 and 7 of the porphyrin, respectively. **c** View of the porphyrin macrocycle and nearby residues on the H263 side of the pocket. **d** View of the porphyrin macrocycle and nearby residues on the M76 side of the pocket. The atoms are represented as sticks and are colored *blue*, *red*, *yellow* and *green* for nitrogen, oxygen, sulfur and carbon, respectively

ring inside the binding pocket versus simulation time is shown in Fig. 6a. The RMSD shows no obvious fluctuations during the simulation time, indicating that the conformation of protoporphyrin does not change dramatically. Compared with the first position, the protoporphyrin ring moves just a little (1.1 Å, reference is the atom N^1 of the protoporphyrin, Fig. 6b).

Model C was built from the E343K variant by adding Fe^{2+} into the center of protoporphyrin. After a 15-ns MD simulation, the enzyme possesses an "open" active site conformation. The cross-section of the upper and lower lip of human ferrochelatase is illustrated in Fig. 3c. Although the lower lip keeps in its original place, the upper lip experiences a large movement, making makes the gap between the two lips larger (from 5 Å to 9 Å, Fig. S3). Compared with the simulation result from model A, the lower lip in model C has no movement. The reason could be ascribed to the binding of protoheme, which captures some residues thus preventing the lower lip from moving. Given a sufficiently long simulation time, the protoheme would be released and the lower lip should have a large movement as in model A. The conserved π-helix is "unwound" from residues 340 to 351 (Fig. 7a), which is consistent with the experimental result of the F110A variant with bound heme, in which the π-helix is unwound from residues 340 to 349 and has a more "open" conformation [36] in comparison to the protoporphyrin-IX-bound structure [15]. As shown in Fig. 6a, the RMSD of the metallation porphyrin reaches ~1.1 Å during the first 50 ps, increases to ~1.2 Å at ~3 ns, and reaches ~1.5 Å in the last part of the MD simulation (from 6 to 15 ns). This result reveals that the metallated porphyrin (heme) has moved during the MD simulation. The direction of movement of heme is out of the active site pocket and the distance moved is 4.0 Å (relative to atom N^1 of the porphyrin, Fig. 6b). Meanwhile, the propionate at position 6 is bent back towards the center of the macrocycle, and forms a hydrogen bond and a salt bridge with residues K118 (2.0 Å) and S303 (3.9 Å), respectively. Here, the figures in brackets are the distance of the hydrogen atom from the donor and the proton acceptor atom; the same notation is used in the following text.

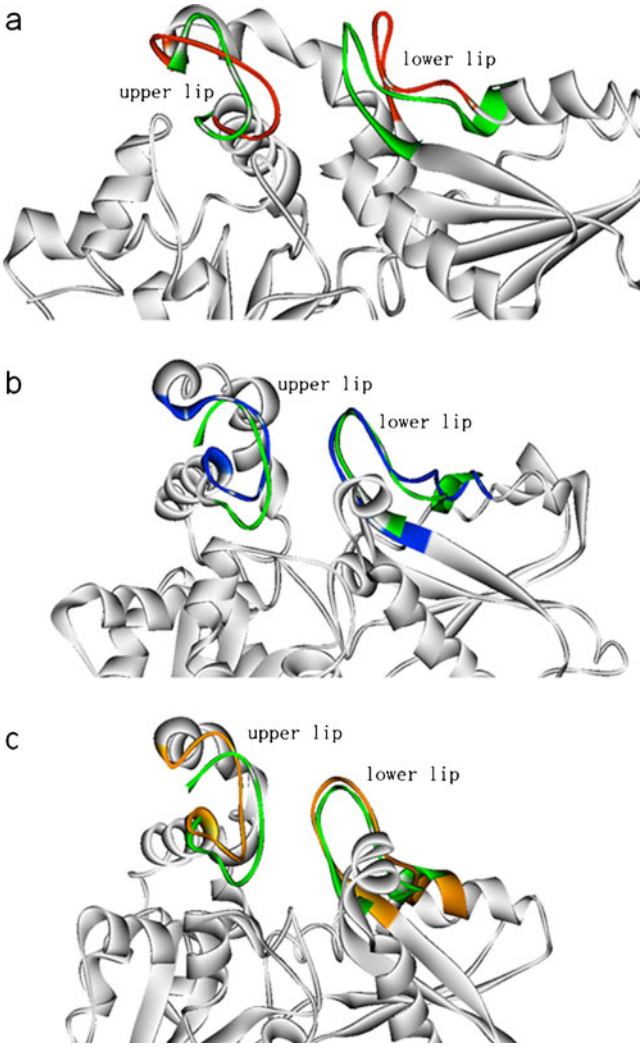

Fig. 3a–c Cross-section of the upper and lower lip of human ferrochelatase. The initial structure is shown in *green*. The structures after MD simulation are shown in red for model A (**a**), *blue* for model B (**b**) and *yellow* for model C (**c**)

Active site structure and hydrogen bond network

The change in conformation of the enzyme could be ascribed to the alteration of the hydrogen bond network and residue orientations. In model A, the imidazole ring of residue H263 rotates by approximately 90° (Fig. 4a). Residues E343 and H341 reorient, and a hydrogen bond is formed between them. The distance between H263 and E343 increases from 3.5 Å to 8.2 Å (measured from the two closest atoms, the same below, Fig. S4). Meanwhile, the side chain of R115 moves closer to E347, and forms hydrogen bonds with the carboxylate group of E347 (from 8.0 to 2.7 Å, Fig. S5). Simultaneously, the distance between the side chain of K118 and E351 decreases from 6.0 to 1.8 Å. Reorientation of side chains also occurs on the opposite side of the active site pocket from H263. As shown in Fig. 4b, M76 moves out of the active site. The rearrangement of M76 enlarges the active site pocket which benefits the insertion of the protoporphyrin IX. The most dramatic change occurs at R164, which rotates more than 90°. The hydrogen bond between R164 and the carboxylate group of D95 breaks (from 2.8 to 8.0 Å, Fig. S6) and the residue D95 moves out of the active site. The new position of R164 is stabilized by hydrogen bonds between the guanido group of R164 and the carboxylate group of E171 (1.68 Å). The obvious change in RMSD of R164 at ~5 ns in Fig. 8 corresponds to these changes in the hydrogen bonds, which lead finally to the transformation from the "closed" to the "open" state.

In model B, H263 shows no obvious movement (Fig. 5a). Both H341 and E343 rotate to some extent. The distance between the side chain of H263 and E343 increases from 2.8 to 6.0 Å (form a salt bridge, Fig. S4) while the distance between H341 and E343 increases from 1.8 to 2.4 Å. However, these conformational changes do not alter the structure of the "wound" π-helix. The protoporphyrin IX is fixed at the active site by R115, S130 and Y123 (see Fig. 2c) and the distances from the closest residues surrounding them are 1.8 Å, 2.1 Å and 1.7 Å, respectively. After MD simulation, there are only a small changes in the distances between protoporphyrin IX and the residues R115 (1.9 Å) and S130 (1.8 Å). A large change occurs on residue Y123, which forms a salt bridge interaction with the propionate at position 7 (3.5 Å). The other residues at the active site pocket have no obvious movement (Fig. 5b).

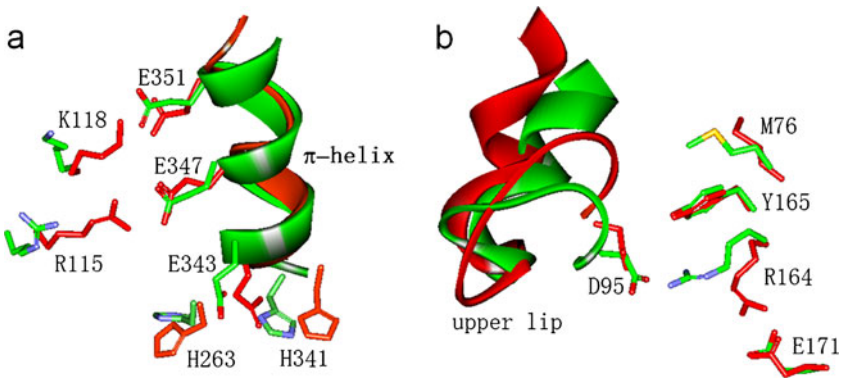

Fig. 4a,b Cartoon representation of the first structure is shown in *green*. The atoms are represented as sticks and are colored *blue*, *red*, *yellow* and *green* for nitrogen, oxygen, sulfur and carbon, respectively. The structure after MD simulation is shown in *red* in model A. **a** Structure of π-helix and key neighbor residues. **b** Structure of upper lip and key neighbor residues

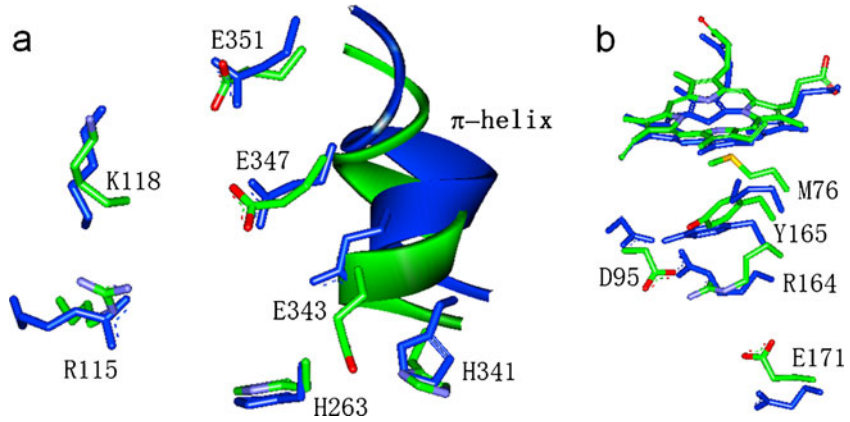

Fig. 5 Cartoon representation of the first structure is shown in *green*. The atoms are represented as sticks and are colored *blue*, *red*, *yellow* and *green* for nitrogen, oxygen, sulfur and carbon, respectively. The structure after MD simulation is shown in *blue* in model B. **a** Structure of π-helix and key neighbor residues. **b** Structure of protoporphyrin and key neighbor residues

In model C, residues H263, H341 and E343 rotate slightly (Fig. 7a). Residue R115 moves out of the active site. The distance between the propionate at position 6 and R115 increases from 2.2 Å to 4.5 Å. Meanwhile, the side chain of K118 rotates to the active site pocket, forming a hydrogen bond with the propionate at position 6 of heme (from 6.8 Å to 2.0 Å). The propionate at position 6 folds back towards the metallated porphyrin and forms a hydrogen bond with S303 (from 6.2 Å to 3.9 Å). At the same time, the residues S130 and Y123 (shown in Fig. 2c,d) rotate slightly and still make hydrogen bonds with the propionate at position 7 (1.8 Å and 2.0 Å, respectively). As shown in Fig. 7b, on the opposite side of the active site pocket from H263, the side chain of M76 rotates out of the active site pocket. The distance between the sulfur atom of M76 and the N^4 atom of porphyrin increases from 3.5 Å to 6.2 Å. The side chain of R164 rotates more than 90° (like model A) and the hydrogen bond with the carboxylate group of D95 is broken (from 2.8 Å to 7.0 Å, Fig. S6). Residue D95 moves out of the active site. The new position of R164 is stabilized by a hydrogen bond with the carboxylate group of E171 (1.9 Å) as in model A. The RMSD of R164 show obvious changes at ~3 ns (Fig. 8) corresponding to these hydrogen bonds changes.

Discussion

As mentioned above, we investigated the change in position of residues H263, H341 and E343 located on one side of the porphyrin that are regarded as involved in proton abstraction from the porphyrin during the process of catalysis [20, 21]. During the simulation process of model A, the imidazole ring of residue H263 rotates and the hydrogen bonds with

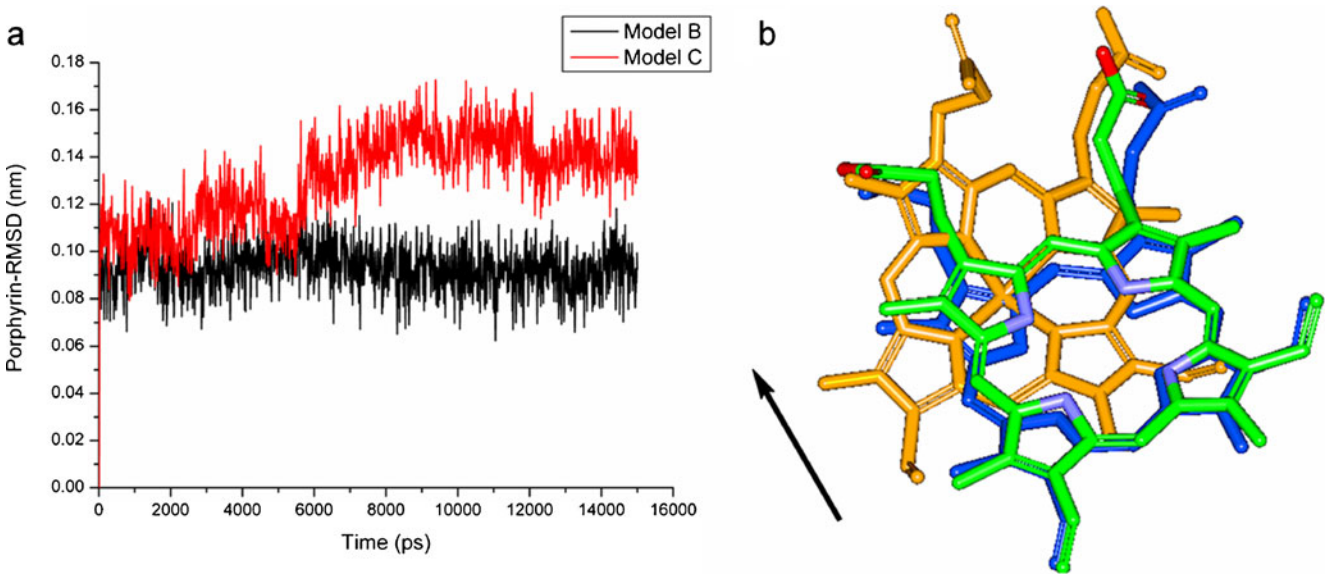

Fig. 6 **a** RMSDs of protoporphyrin (*black*) and heme (*red*) versus simulation time. **b** The first structure of protoporphyrin is represented in stick form and is colored *green*. The atoms are colored *blue*, *red* and *green* for nitrogen, oxygen and carbon, respectively. The structures after MD simulation are shown in blue for model B (protoporphyrin) and for model C *yellow* (heme). *Arrow* Direction of heme movement

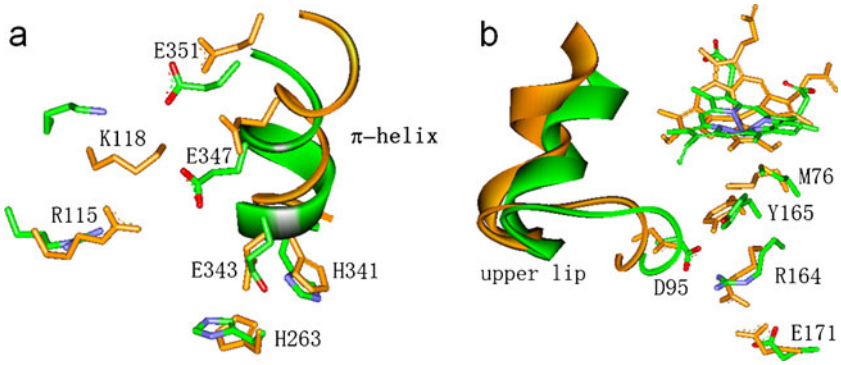

Fig. 7a,b Cartoon representation of the first structure is shown in *green*. The atoms are represented as sticks and are colored *blue*, *red*, *yellow* and *green* for nitrogen, oxygen, sulfur and carbon, respectively. The structure after MD simulation is shown in yellow in model C. **a** Structure of π-helix and key neighbor residues. **b** Structure of upper lip and key neighbor residues

E343 and one pyrrole proton of the porphyrin (Fig. 4a) are broken. Both H341 and E343 experience large movement. The conformation of the π-helix is "unwound". In model B, E343 rotates to a large degree while both H263 and H341 show little change, which elongates the distance between H263 and E343 (Fig. 5a). The π-helix is in a "wound" state. For model C (with metallated porphyrin), unlike model A, residues H263, H341 and E343 rotate to only a small degree (Fig. 7a). However, the π-helix can be in an "unwound" state like that of model A. These positional changes reveal that the reorientations of residues H263, H341 and E343 do not relate directly to the conformation of the π-helix, although H341 and E343 are located on the π-helix.

So, what are the key residues controlling the change in π-helix conformation from "wound" to "unwound"? For models A and C, in which the π-helix is "unwound", residues E347 and E351 can form hydrogen bonds with R115 and K118, respectively. However, for model B, in which the π-helix is in the "wound" state, there are no hydrogen bonds between these residues. Unlike the positions of residues H263, H341 and E343, residues R115 and K118 sit at the side of the π-helix. The formation of hydrogen bonds with residue E347 and E351 will exert a pull force on the π-helix

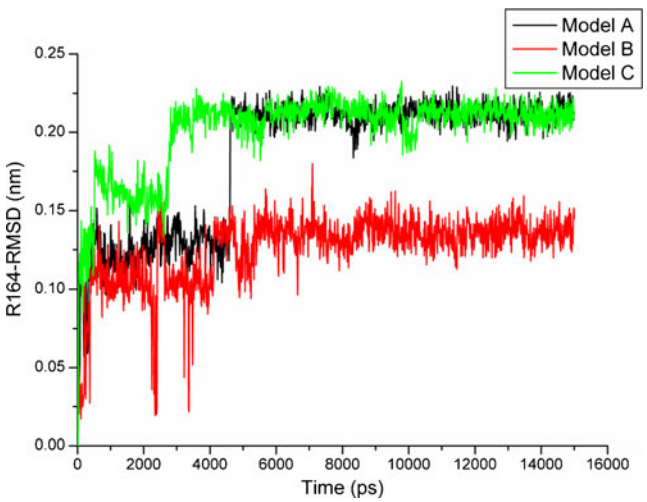

Fig. 8 RMSD of residue R164 for the CA, C, N atoms in the 15 ns MD simulations

to make the other residues located on the π-helix reorient by steric effect, inducing alteration of the hydrogen bond network of the π-helix, finally "unwinding" the π-helix.

The side chains of M76 and R164 move closely toward the protoporphyrin IX when it is captured by the enzyme. However, after ferrous ion is imported into the porphyrin, residues M76 and R164 rotate away from the metallated product. The reason for this movement of M76 could be ascribed to the weakened electrostatic interaction between the methyl group on M76 and the center N atoms of the porphyrin after Fe^{2+} is pulled into the center of the porphyrin. The flexibility of residues M76 and R164 probably make them act as tools to play the role of transporting ferrous ion. The ferrous ion insertion process has been described previously in human ferrochelatase [10, 20] and in yeast [23], in which it was proposed that Fe^{2+} is transported from the exterior of the enzyme at D383/H231 via residues W227 and Y191 to the site of metallation at residues R164. Our QM/MM calculation gave the same result, i.e., that the insertion pathway of Fe^{2+} into the protoporphyrin IX is easier from the M76 side than from the H263 side . However, in *Bacillus subtilis* ferrochelatase, the insertion path of Fe^{2+} is from the opposite side [13, 19].

Protoporphyrin is stabilized at the active site by forming hydrogen bonds with residues R115, Y123 and S130. This pattern is very similar to Szefczyk's MD simulation results on mouse ferrochelatase [37]. After ferrous ion is imported into the protoporphyrin, residue M76 moves away from the heme while residues Y165 and R164 move out of the active site. The hydrogen bond between the guanido group of R164 and the carboxylate group of D95 is broken (RMSD shows an obvious change at ~3 ns, Fig. 8), which promotes movement of residues 90–115 out of the active site. Thus, the active site is in the "open" state.

The electronegativity of the oxygen in the propionate at position 6 is decreased (the calculated ESP charge changes from −0.71 to −0.60) after the Fe^{2+} is introduced, which weakens the hydrogen bond between the oxygen and R115 making it easier to break. Therefore, the simulation result shows that the hydrogen bond is broken and R115 rotates out of the active site. At the same time, the side chain of

K118 rotates to the active site pocket, forming a hydrogen bond with the propionate at position 6 of heme. This alternating of the two hydrogen bonds promotes movement of the heme out of the active center (RMSD increases to ~1.2 Å at ~3 ns, Fig. 6a). Furthermore, the propionate at position 6 folds back towards the metallated porphyrin, forming a hydrogen bond and a salt bridge interaction with S303 and E347, respectively. This series of hydrogen bond realignments accelerates movement of heme out of the active site. The RMSD of heme increases to ~1.5 Å (Fig. 6a). Meanwhile, residues E347 and E351 located on the π-helix form an acidic path resulting in a salt bridge interaction with the propionate of the heme, which will facilitate the release of metallated porphyrin.

It has been suggested that the metallation in ferrochelatase involves distortion of the protoporphyrin [18, 33, 37]. In the crystal structure of E343K variant (2HRE), the protoporphyrin is completely planar. In our simulation results of model B, the protoporphyrin was distorted, with the pyrrole nitrogen atom bent toward the direction of residue MET 76, which benefits the insertion of Fe^{2+} from the side of M76. However, after the ferrous ion has been imported to the porphyrin, the resulting changes in hydrogen bonds of the heme propionate with neighboring residues distorts the porphyrin ring quite a lot . At the same time, the changes in the hydrogen bond network facilitate the release of the heme.

Based on the above results, we propose that the catalysis process follows the procedure illustrated in Fig. 9: first, the

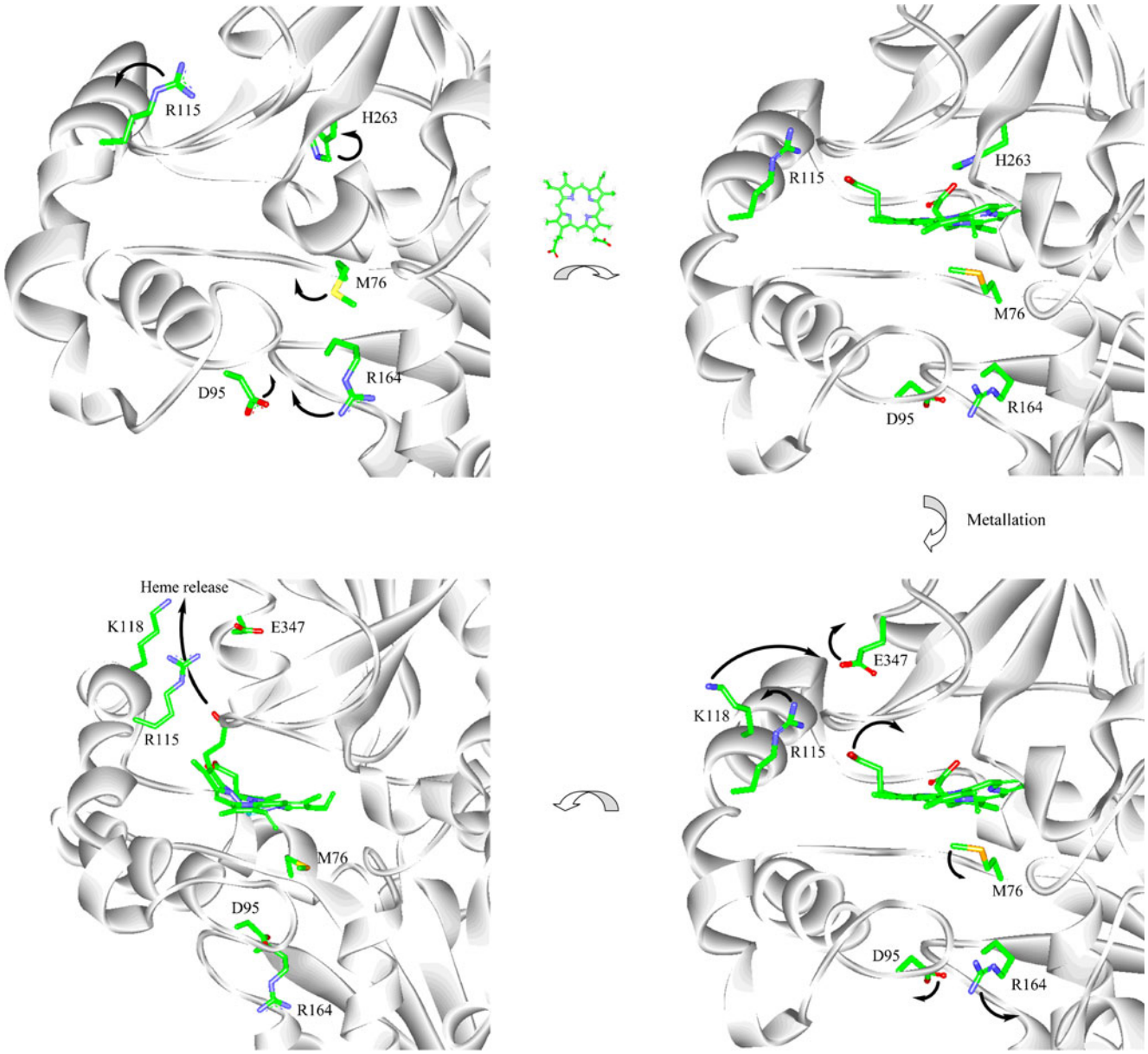

Fig. 9 Proposed catalytic process for human ferrochelatase and the role of the key residues

enzyme has an open "mouth". Following binding of ferrous ion in the active site, the protoporphyrin approaches the active site pocket. H263 rotates to form hydrogen bonds with E343 and one pyrrole proton of the porphyrin. The protoporphyrin IX is fixed at the active site by R115, S130 and Y123. M76 rotates into the active site pocket. R164 rotates and forms a hydrogen bond with D95. The active site is now closed. Next, the protons on the porphyrin are extracted by H263 [20, 21]. The ferrous ion enters the porphyrin. Then, M76 moves away from the heme. The hydrogen bond between R164 and D95 is broken, which induces residues 90–115 to move out. The "mouth" of the enzyme is open, which facilitates movement of the heme out of the active site. The propionate at position 6 of heme folds back towards the metallated porphyrin and forms hydrogen bonds with K118 and S303 and a salt bridge interaction with E347, which accelerates heme release. In this process, alterations in the hydrogen bond network and the positions of E347 and E351 lead to structural rearrangements of the π-helix by both steric effects and hydrogen bonding. Residue R164 acts as a signal indicating the active site conformation of enzyme. When R164 forms a hydrogen bond with D95, the active site is closed, while a hydrogen bond with E171 indicates that the active site is open.

Conclusions

Our MD simulations provide insight into the conformational movements and function of the active site residues of human ferrochelatase. Based on these data, the simulation process of model A can be regarded as the reverse process of protoporphyrin insertion. A series of hydrogen bond realignments trigger reshaping of the active site, which facilitates the insertion of ferrous ion and protoporphyrin. The simulation of model B shows the steady closed state of the enzyme with protoporphyrin before metallation. The simulation process of model C shows the process of heme release with the mouth from "closed" to "open" state. The "open" and "closed" conformations obtained by the simulations are in agreement with the corresponding crystal structures. Residue R164 acts as a signal showing alteration of the active site conformation. When R164 forms a hydrogen bond with D95, the active site is closed; a hydrogen bond with E171 indicates that the active site is open. The conformational change of the π-helix is related to the alteration of the hydrogen bond and the positions of E347 and E351. The alteration of the hydrogen bonds between the propionate of the heme with R115, K118 and S303 trigger movement of heme out of the active site. In addition, residues E347 and E351 located on the π-helix, form an acidic path leading to a salt bridge interaction with the propionate of the heme, accelerating the release process.

Acknowledgments This research was supported by the National Natural Science Foundation of the People's Republic of China (No. 90608012, No. J1103305), the High Performance Grid Computing Platform of SunYat-sen University, the Guangdong Province Key Laboratory of Computational Science and the Guangdong Province Computational Science Innovative Research Team.

References

1. Dailey HA, Dailey TA (2003) Ferrochelatase. In: Kadish KM, Smith KM, Guilard R (eds) The porphyrin handbook, vol 12. Elsevier, Irvine, CA, pp 93–121
2. Dailey HA (2002) Terminal steps of haem biosynthesis. Biochem Soc Trans 30:590–595
3. Magnus IA, Jarrett A, Prankerd TA, Rimington C (1961) Erythropoietic protoporphyria. A new porphyria syndrome with solar urticaria due to protoporphyrinaemia. Lancet 2:448–451
4. Chen FP, Risheg H, Liu YY, Bloomer J (2002) Ferrochelatase gene mutations in erythropoietic protoporphyria: focus on liver disease. Cell Mol Biol 48:83–89
5. Sassa S, Zalar GL, Poh-Fitzpatrick MB, Anderson KE, Kappas A (1982) Studies in porphyria: functional evidence for a partial deficiency of ferrochelatase activity in mitogen-stimulated lymphocytes from patients with erythropoietic protoporphyria. J Clin Invest 69:809–815
6. Baum SJ, Plane RA (1966) Kinetics of the incorporation of magnesium(II) into porphyrin1. J Am Chem Soc 88:910–913
7. Daily HA, Fleming JE (1983) Bovine ferrochelatase. Kinetic analysis of inhibition by N-methylprotoporphyrin, manganese, and heme. J Biol Chem 258:11453–11459
8. Lavallee DK (1985) Kinetics and mechanisms of metalloporphyrin reactions. Coord Chem Rev 61:55–96
9. Inamo M, Kamiya N, Inada Y, Nomura M, Funahashi S (2001) Structural characterization and formation kinetics of sitting-atop (SAT) complexes of some porphyrins with copper(II) ion in aqueous acetonitrile relevant to porphyrin metalation mechanism. Structures of aquacopper(II) and Cu(II)-SAT complexes as determined by XAFS spectroscopy. Inorg Chem 40:5636–5644
10. Sellers VM, Wu CK, Dailey TA, Dailey HA (2001) Human ferrochelatase: characterization of substrate-iron binding and proton-abstracting residues. Biochemistry 40:9821–9827
11. Funahashi S, Inada Y, Inamo M (2001) Dynamic study of metal-ion incorporation into porphyrins based on the dynamic characterization of metal ions and on sitting-atop complex formation. Anal Sci 17:917–927
12. Shen Y, Ryde U (2005) Reaction mechanism of porphyrin metallation studied by theoretical methods. Chem Eur J 11:1549–1564
13. Hansson MD, Karlberg T, Rahardja MA, Al-Karadaghi S, Hansson M (2007) Amino acid residues His183 and Glu264 in *Bacillus subtilis* ferrochelatase direct and facilitate the insertion of metal ion into protoporphyrin IX. Biochemistry 46:87–94
14. Medlock A, Swartz L, Dailey TA, Dailey HA, Lanzilotta WN (2007) Substrate interactions with human ferrochelatase. Proc Natl Acad Sci USA 104:1789–1793
15. Medlock AE, Dailey TA, Ross TA, Dailey HA, Lanzilotta WN (2007) A pi-helix switch selective for porphyrin deprotonation and product release in human ferrochelatase. J Mol Biol 373:1006–1016
16. Dailey HA, Wu CK, Horanyi P, Medlock AE, Najahi-Missaoui W, Burden AE, Dailey TA, Rose J (2007) Altered orientation of active site residues in variants of human ferrochelatase. Evidence for a hydrogen bond network involved in catalysis. Biochemistry 46:7973–7979

17. Hoggins M, Dailey HA, Hunter CN, Reid JD (2007) Direct measurement of metal ion chelation in the active site of human ferrochelatase. Biochemistry 46:8121–8127
18. Karlberg T, Hansson MD, Yengo RK, Johansson R, Thorvaldsen HO, Ferreira GC, Hansson M, Al-Karadaghi S (2008) Porphyrin binding and distortion and substrate specificity in the ferrochelatase reaction: the role of active site residues. J Mol Biol 378:1074–1083
19. Wang YX, Shen Y, Ryde U (2009) QM/MM study of the insertion of metal ion into protoporphyrin IX by ferrochelatase. J Inorg Biochem 103:1680–1686
20. Wu CK, Dailey HA, Rose JP, Burden A, Sellers VM, Wang BC (2001) The 2.0 angstrom structure of human ferrochelatase, the terminal enzyme of heme biosynthesis. Nat Struct Biol 8:156–160
21. Gora M, Grzybowska E, Rytka J, Labbe-Bois R (1996) Probing the active-site residues in *Saccharomyces cerevisiae* ferrochelatase by directed mutagenesis. J Biol Chem 271:11810–11816
22. Meyer E (1992) Internal water molecules and H-bonding in biological macromolecules: a review of structural features with functional implications. Protein Sci 1:1543–1562
23. Lange H, Kispal G, Lill R (1999) Mechanism of iron transport to the site of heme synthesis inside yeast mitochondria. J Biol Chem 274:18989–18996
24. Medlock AE, Carter M, Dailey TA, Dailey HA, Lanzilotta WN (2009) Product release rather than chelation determines metal specificity for ferrochelatase. J Mol Biol 393:308–319
25. Genheden S, Diehl C, Akke M, Ryde U (2010) Starting-condition dependence of order parameters derived from molecular dynamics simulations. J Chem Theory Comput 6:2176–2190
26. Karplus M (2003) Molecular dynamics of biological macromolecules: a brief history and perspective. Biopolymers 68:350–358
27. Karplus M, McCammon JA (2002) Molecular dynamics simulations of biomolecules. Nat Struct Biol 9:646–652
28. Zhang J, Xu YC, Shen JH, Luo XM, Chen JG, Chen KX, Zhu WL, Jiang HL (2005) Dynamic mechanism for the autophosphorylation of CheA histidine kinase: molecular dynamics simulations. J Am Chem Soc 127:11709–11719
29. Weiner SJ, Kollman PA, Nguyen DT, Case DA (1986) An all atom force field for simulations of proteins and nucleic acids. J Comput Chem 7:230–252
30. Weiner SJ, Kollman PA, Case DA, Singh UC, Ghio C, Alagona G, Profeta S, Weiner P (1984) A new force field for molecular mechanical simulation of nucleic acids and proteins. J Am Chem Soc 106:765–784
31. Cornell WD, Cieplak PI, Bayly CI, Gould IR, Merz KM, Ferguson DM, Spellmeyer DC, Fox T, Caldwell JW, Kolman PA (1995) J Am Chem Soc 117:5179–5197
32. Ahlrichs R, Bär M, Häser M, Horn H, Kölmel C (1989) Electronic structure calculations on workstation computers: the program system turbomole. Chem Phys Lett 162:165–169
33. Sigfridsson E, Ryde U (2003) The importance of porphyrin distortions for the ferrochelatase reaction. J Biol Inorg Chem 8:273–282
34. Humphrey W, Dalke A, Schulten K (1996) VMD: visual molecular dynamics. J Mol Graph 14:33–38
35. Wlodek ST, Clark TW, Scott R, McCammon JA (1997) Molecular dynamics of acetylcholinesterase dimer complexed with tacrine. J Am Chem Soc 119:9513–9522
36. Fodje MN, Al-Karadaghi S (2002) Occurrence, conformational features and amino acid propensities for the pi-helix. Protein Eng 15:353–358
37. Szefczyk B, Cordeiro MNDS, Franco R, Gomes JANF (2009) Molecular dynamics simulations of mouse ferrochelatase variants: what distorts and orientates the porphyrin? J Biol Inorg Chem 14:1119–1128